Hindawi Publishing Corporation
Mathematical Problems in Engineering
Volume 2014, Article ID 208019, 12 pages
http://dx.doi.org/10.1155/2014/208019

Research Article

Robust H_2/H_∞ Control for the Electrohydraulic Steering System of a Four-Wheel Vehicle

Min Ye, Quan Wang, and Shengjie Jiao

Highway Maintenance Equipment National Engineering Laboratory, Chang'an University, Xi'an 710064, China

Correspondence should be addressed to Min Ye; mingye@chd.edu.cn

Received 27 March 2014; Accepted 18 June 2014; Published 20 July 2014

Academic Editor: Xing-Gang Yan

To shorten the steer diameter and to improve the maneuverability flexibility of a construction vehicle, four wheels' steering system is presented. This steering system consists of mechanical-electrical-hydraulic assemblies. Its diagram and principle are depicted in detail. Then the mathematical models are derived step by step, including the whole vehicle model and the hydraulic route model. Considering the nonlinear and time-varying uncertainty of the steering system, robust H_2/H_∞ controller is put forward to guarantee both the system performance and the robust stability. The H_∞ norm of the sensitive function from the parameter perturbation of the hydraulic system to the yaw velocity of the vehicle is taken as the evaluating index of the robustness and the H_2 norm of the transfer function from the external disturbance to the steering angle of the wheel as the index of linear quadratic Gaussian. The experimental results showed that the proposed scheme was superior to classical PID controller and can guarantee both the control performance and the robustness of the steering system.

1. Introduction

Traditionally a wheel vehicle is steered by two front wheels or by two rear wheels, which is controlled by a driver's steering wheel. The shortage of the two wheels' steering system is that the steering diameter is large, and it is not easy to satisfy steering requirement under narrow space, which constrict its application, especially for a large and heavy-duty construction vehicle. To improve the direction maneuverability and stability during the driving, furthermore to improve the safety and comfort, four wheels' steering (4WS) system is studied recently. 4WS systems for automobiles have been actively studied to improve the maneuverability of vehicles at low speeds and enhance their stability at high speeds. Many automobile companies had developed concept vehicles with 4WS system, for example, Honda, Nissan, and Mazda [1, 2]. Borrowing the idea from the automobile industry, 4WS has been applied in the construction vehicle, for example the concrete spreading machine "SF-3004" from CMI Terex Company and ditch cutter "560" from Case Company [3]. The uncertainty of a construction vehicle is more serious than of a car, which has a large power hydraulic system and works in bad and dirty environment.

The control of the 4WS system is complicated and sometimes may not be effective due to the nonlinear characteristics and unknown environmental parameters. During the last 20 years, many different control methods have been applied on 4WS system [4–6]. Early for a 4WS vehicle, a simple speed-dependent ratio between rear and front wheels has been used in an open-loop controller to achieve a zero constant sideslip angle during directional maneuvers [7]. Ackermann and Sienel [8] used a proportional controller in their nonlinear 3 DOF (degrees of freedom) model, while Ji et al. [9] used proportional and compensator controllers in their control strategy. Lv et al. [10] and You and Chai [11] used fuzzy logic method to investigate the performance on controlling the wheel angle, and they did not give out the experimental validation. With the development of sliding mode control [12, 13], it has been applied to control four-wheel vehicle [14]. However it should be noted that the aforementioned controllers are based on the fairly concise model, where the uncertainty is not considered. The parameters of a construction vehicle are subject to a vast range of uncertainties such as external disturbances, unmodeled dynamics, road roughness, wind gusts, load fluctuations, and braking/accelerating forces. Thus, a serious robust stability problem for the 4WS

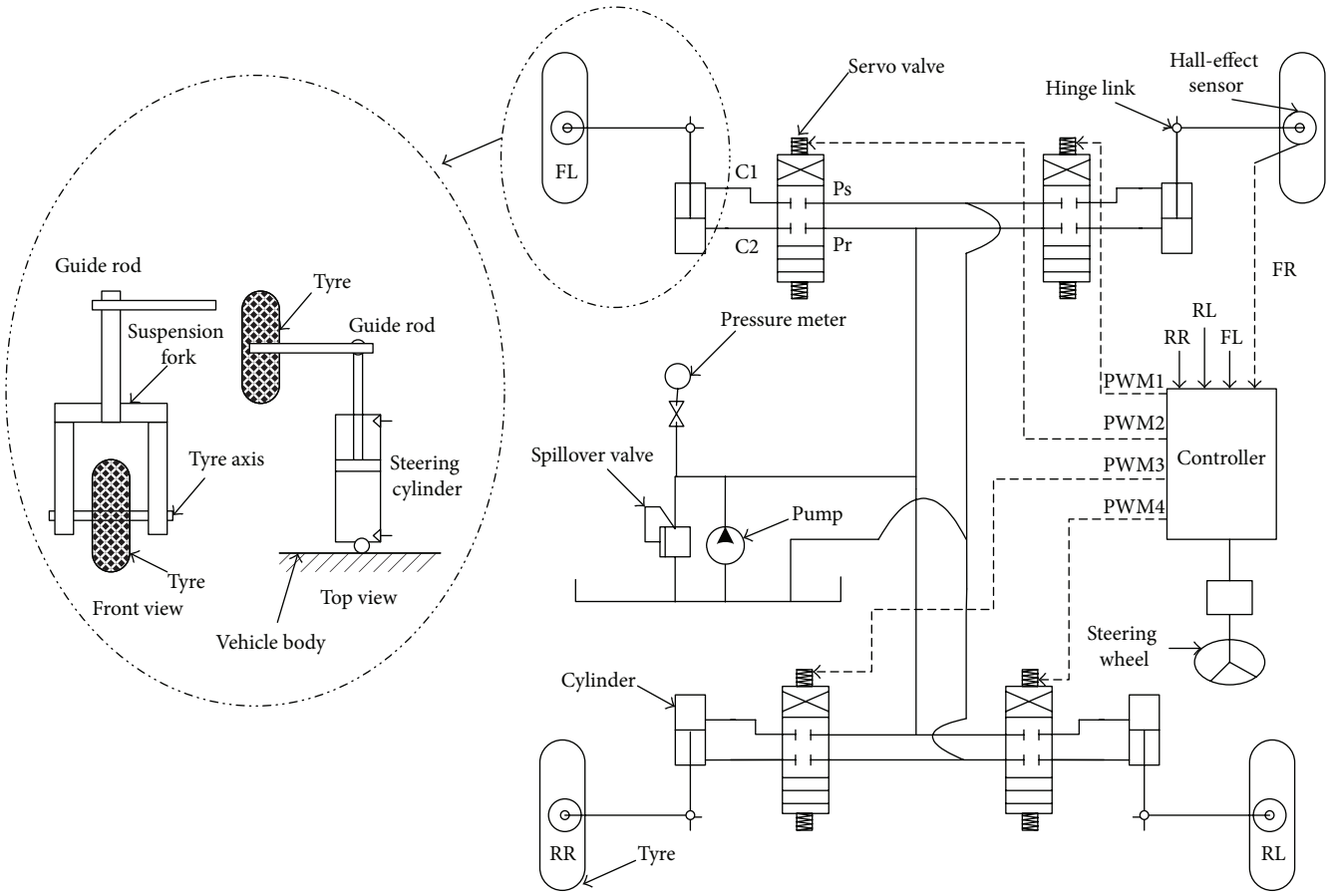

Figure 1: Schematic diagram of 4WS vehicle.

vehicle control has been raised; namely, the vehicle controller has to cope with these uncertainties to keep maneuvering stability and ensure that the system performance does not deteriorate too much. With the uncertainty the linear design model cannot express the exact behavior, which is usually required for the controller design. So that the classical control method is ineffective to guarantee the control performance. Robust H_2/H_∞ control has been proven to be effective for controls related to nonlinear dynamic systems, which is robust to uncertainty. In [15], a LMI approach to the robust state feedback H_∞ control for linear discrete singular systems with norm-bounded uncertainty was developed. The robust H_∞ controller design algorithm was presented and an explicit expression for the desired state feedback control law was also given [16].

So it can be concluded that the benefits of a 4WS system are often described but not quantified, and most of the studies carry out only the simulations not the experiments. This paper reviews the purposes, methods, and advantages of 4WS; firstly, the uncertainty model is put forward and secondly the robust H_2/H_∞ controller is designed to attenuate the parameter perturbation and the outside disturbance of the steering system. Furthermore experiments are carried out. Finally the conclusions are summarized.

2. The Diagram of the 4WS Vehicle

To realize the function of 4WS for a construction vehicle, the drive-by-wire hydraulic system is proposed, as shown in Figure 1, which includes a hydraulic pump, an electrohydraulic servo valve, a hydraulic cylinder, and a controller. The hydraulic cylinder is connected to the wheel by the traditional double suspension fork guidance mechanism, as shown in the dotted line of Figure 1, which includes the planar mechanism of 4WS from front view and top view. The cylinder rod propels the suspension fork and furthermore steers the wheel to the desired angle. The hydraulic cylinder of each wheel is connected in parallel to hydraulic route to propel the four wheels, preventing them from interfering with each other. The pressure of the pump is set up by the spillover valve and keeps constant during running. The controller acquaints the command signal from the driver's steering wheel and output PWM control signals for each electrohydraulic servo valve. The PWM signal is proportional to the flow rate running into the cylinder. Provided that the hydraulic flow cannot be compressed, the displacement of the cylinder rod is proportional to the PWM signals. The steer degree of the wheel is controlled by the controller indirectly.

For a wheel vehicle, the requirements for the steering system are high following accuracy, quick response velocity, and

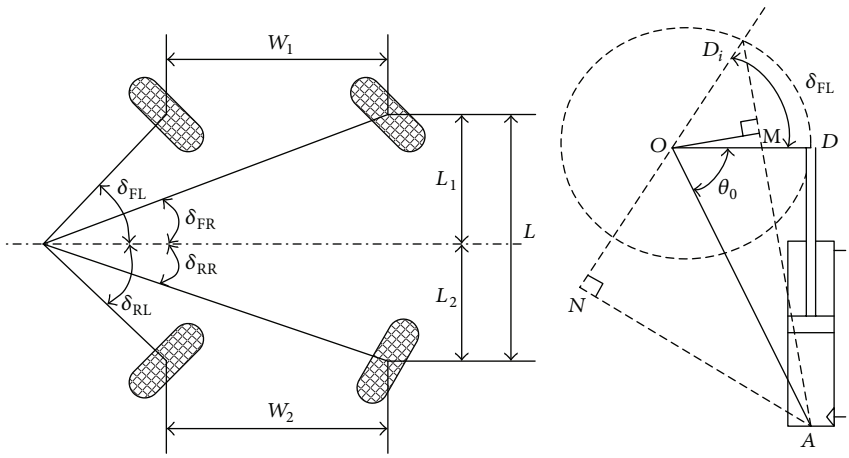

(a) The Ackerman steering triangle diagram

(b) The mathematical diagram of a steering wheel

Figure 2: Ackerman steering triangle diagram.

good stability. For a construction vehicle, which is running at serious condition, good disturbance attenuation ability is extra required. To shorten the power consumption, tire wear, and ground friction and to improve maneuverability flexibility of a wheel vehicle during steering and running, it is better that all the wheels roll only on the ground without producing any sliding (including side sliding, longitudinal sliding, and slippage). There are three kinds of steer modes for a construction vehicle: two front wheels' steering, four wheels' steering, and sideways steering modes. The Ackerman steer triangle is shown in Figure 2(a). At front wheel steering mode, the steering centerline lies in the rear wheel axis and the steering angles of the rear wheels are 0 degrees. At four wheels' steering mode, the steering centerline is in the middle of front and rear axles. The steering directions of the front wheels are contrary to those of rear wheels. At sideways steering mode, the steering directions of four wheels are the same, and there is no steering centerline.

The relationship between the rod of the hydraulic cylinder and the steering wheel is shown in Figure 2(b). Without any input signal from the steering wheel, the cylinder rod locates at initial position AD. When the wheel steering angle is δ, the rod locates at AD_i. The distance between AD_i is expressed as $\overline{AD_i}$. Because $\Delta MOD_i \backsim \Delta NAD_i$, so $\overline{D_iO}/\overline{AD_i} = \overline{MO}/\overline{AN}$. Assume that $\overline{D_iO} = r$, $\overline{AO} = L$; we can get that

$$\begin{aligned} \overline{AN} &= L \cdot \sin\left(\delta + \theta_0\right), \\ \overline{MO} &= \frac{L \cdot r \cdot \sin\left(\delta + \theta_0\right)}{\overline{AD_i}}, \end{aligned} \tag{1}$$

where $\theta = \arcsin(r/L)$ is the angle between OD and AO, δ is the steering angle of the wheel. According to the cosine theory, the length between two joints can be expressed as

$$\overline{AD_i} = \sqrt{L^2 + r^2 - 2 \cdot L \cdot r \cdot \cos\left(\alpha + \delta\right)}. \tag{2}$$

We can get that

$$\delta = \arccos \frac{\left(Y + y\right)^2 - L^2 - r^2}{2 \cdot r * L} - \alpha, \tag{3}$$

where Y is the initial length of the cylinder when the steering angle is 0 degrees. y is the stretching length of the cylinder rod, and $Y^2 = L^2 - r^2$.

The relationships between two front wheels are as follows at front wheel steering mode:

$$\begin{aligned} ctg\left(\delta_{FL}\right) - ctg\left(\delta_{FR}\right) &= \frac{W_1}{L}, \\ \delta_{RL} = \delta_{RR} &= 0. \end{aligned} \tag{4}$$

The relationships between the four front wheels are shown as follows at four wheels' steering mode:

$$\begin{aligned} ctg\left(\delta_{FL}\right) - ctg\left(\delta_{FR}\right) &= \frac{W_1}{L_1}, \\ ctg\left(\delta_{RL}\right) - ctg\left(\delta_{RR}\right) &= \frac{W_2}{L_2}, \\ \delta_{FL} = \delta_{RL}&. \end{aligned} \tag{5}$$

The relationships between the four wheels are shown as follows at sideways steering mode:

$$\delta_{FL} = \delta_{FR} = \delta_{RL} = \delta_{RR}, \tag{6}$$

where, in the above equations, δ_{FR} and δ_{FL} are steer angles of FL (front left) or FR (front right) wheel. δ_{RL} and δ_{RR} are steer angles of RL (rear left) or RR (rear right) wheel; W_1, W_2 are distances between two front or rear wheels; L_1, L_2 are the distances from front axle or rear axle to steer centerline; L is the distance from front axle to rear axle. The structure parameters of the steering system are shown in Table 1.

Table 1: Structure parameters of the 4ws system (unit: m).

W_1	W_2	L_1	L_2	L
1.3	1.3	1.3	1.7	3

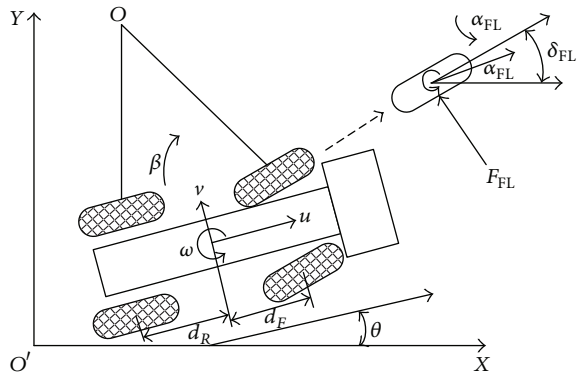

Figure 3: The diagram of the 4WS vehicle.

3. Mathematical Models of the 4WS Vehicle

There are two parts for the models. One is the whole vehicle model and the other is the hydraulic route model. The former aims at the yaw velocity dynamic response of the whole vehicle. The latter consists of the controller, the electrohydraulic servo valve, the hydraulic cylinder, and the wheel.

3.1. The Dynamic Vehicle Model. The dynamic vehicle model is shown in Figure 3, where β is the slip angle of the vehicle, ω is the yaw velocity, v is the lateral velocity, and u is the forward velocity. F_{IJ} ($I = F$ or R; $J = L$ or R) is the lateral force of different wheel. δ_{IJ} is the steer angle of different wheel, δ_I is the equivalent steer angle $\delta_I = (\delta_{IR} + \delta_{IL})/2$, and α_{IJ} is the slip angle of different wheel. θ is the angle between the longitudinal center line of the vehicle and the coordinate X. d_F and d_R are the distance from the mass center of the vehicle to the front and rear axles [17].

The motion differential equation of the vehicle can be expressed as

$$\begin{aligned} m(\dot{v} + u\omega) &= k_{FL}\alpha_{FL} + k_{FR}\alpha_{FR} + k_{RL}\alpha_{RL} + k_{RR}\alpha_{RR}, \\ I_z\dot{\omega} &= d_1k_{FL}\alpha_{FL} + d_1k_{FR}\alpha_{FR} + d_2k_{RL}\alpha_{RL} + d_2k_{RR}\alpha_{RR}, \end{aligned} \tag{7}$$

where k_{IJ} is cornering stiffness coefficient of different wheel, $I = F$ or R represents the front or rear axle, and $J = L$ or R represents the left or right wheel. m is the vehicle mass, I_z is the yaw inertia moment, and, for other parameters, one can refer to Figure 3. If the steer angle δ_I and the slip angle of the mass center β are small enough, we can assume that $\beta \doteq v/u$, so (1) can be simplified as

$$\begin{aligned} \alpha_{IL} &= \frac{(v - d_I\omega)}{u} - \delta_{IL} = \beta - \frac{d_I\omega}{u} - \delta_{IL} \quad I = F, R, \\ \alpha_{JR} &= \frac{(v - d_J\omega)}{u} - \delta_{JR} = \beta - \frac{d_J\omega}{u} - \delta_{JR} \quad J = F, R. \end{aligned} \tag{8}$$

At the same time we can get that $\delta_I = (\delta_{IL} + \delta_{IR})/2$. If we assume that $k_I = (k_{IL} + k_{IR})/2$, according to (7) and (8), it can be concluded that

$$\begin{aligned} m(\dot{v} + u\omega) &= 2(k_F + k_R)\beta + 2\frac{\omega}{u}(k_Fd_F - k_Rd_R) \\ &\quad - 2(k_F\delta_F + k_R\delta_R), \\ I_z\dot{\omega} &= 2(k_Fd_F - k_Rd_R)\beta + 2\frac{\omega}{u}\left(k_Fd_F^2 + k_Rd_R^2\right) \\ &\quad - 2(k_Fd_F\delta_F - k_Rd_R\delta_R). \end{aligned} \tag{9}$$

In (9), $\beta = v/u$, where if u is a constant value, it can be derivated that $\dot{\beta} = \dot{v}/u$. The state equation of the vehicle can be gotten as

$$\begin{aligned} \dot{x} = \begin{bmatrix} \dot{\beta} \\ \dot{\omega} \end{bmatrix} &= \begin{bmatrix} \dfrac{2(k_F + k_R)}{mu} & \dfrac{2(k_Fd_F - k_Rd_R)}{mu^2} - 1 \\ \dfrac{2(k_Fd_F - k_Rd_R)}{I_z} & \dfrac{2\left(k_Fd_F^2 + k_Rd_R^2\right)}{I_zu} \end{bmatrix} \\ &\quad \times \begin{bmatrix} \beta \\ \omega \end{bmatrix} + \begin{bmatrix} \dfrac{-2k_F}{mu} & \dfrac{-2k_R}{mu} \\ \dfrac{-2d_Fk_F}{I_z} & \dfrac{-2d_Rk_R}{I_z} \end{bmatrix} \times \begin{bmatrix} \delta_F \\ \delta_R \end{bmatrix}, \end{aligned} \tag{10}$$

where the state vector is $x = [\beta \ \ \omega]^T$ and the input vector is $U = [\delta_F \ \ \delta_R]$.

According to state equation (10) and derivate equation (10), we can get the second-order differential equation as

$$\begin{aligned} &\ddot{\omega} - \left(\frac{2DI_z + 2Bm}{mI_zu}\right)\dot{\omega} + \left(\frac{4DB - 2EA}{mu^2I_z}\right)\omega \\ &\quad = F_1\dot{\delta}_1 + \left(\frac{2EmuG - 2F_1I_zD}{muI_z}\right)\delta_1, \end{aligned} \tag{11}$$

where $E = C/2$, $F_1 = -2(k_1d_1 - k_2d_2k_a)/I_z$, $G = -2(k_1 + k_2k_a)/mu$, $H = -((2DI_z + 2Bm)/mI_zu)$, $M = (4DB - 2EA)/mu^2I_z$, $B_0 = (2EmuG - 2F_1I_zD)/muI_z$, and $B_1 = F_1$.

The equation can be simplified further as

$$\ddot{\omega} + H\dot{\omega} + M\omega = B_1\dot{\delta}_1 + B_0\delta_1. \tag{12}$$

So by the natural frequency $\omega_0^2 = M$ and the subsidence $2\omega_0\xi = H$, we can get the solution of (12) as

$$\begin{aligned} \omega(t) &= \frac{B_0\delta_0}{\omega_0^2} + A_1e^{-\xi\omega_0t}\cos\left(\omega_0\sqrt{1 - \xi^2} * t\right) \\ &\quad + A_2e^{-\xi\omega_0t}\sin\left(\omega_0\sqrt{1 - \xi^2} * t\right). \end{aligned} \tag{13}$$

Supposed that the input angle δ_1 is a step input, which can be shown in (14)

$$\begin{aligned} \delta_1 &= 0, \quad t < 0, \\ \delta_1 &= \delta_0, \quad t \geq 0, \\ \dot{\delta}_1 &= 0, \quad t > 0, \end{aligned} \tag{14}$$

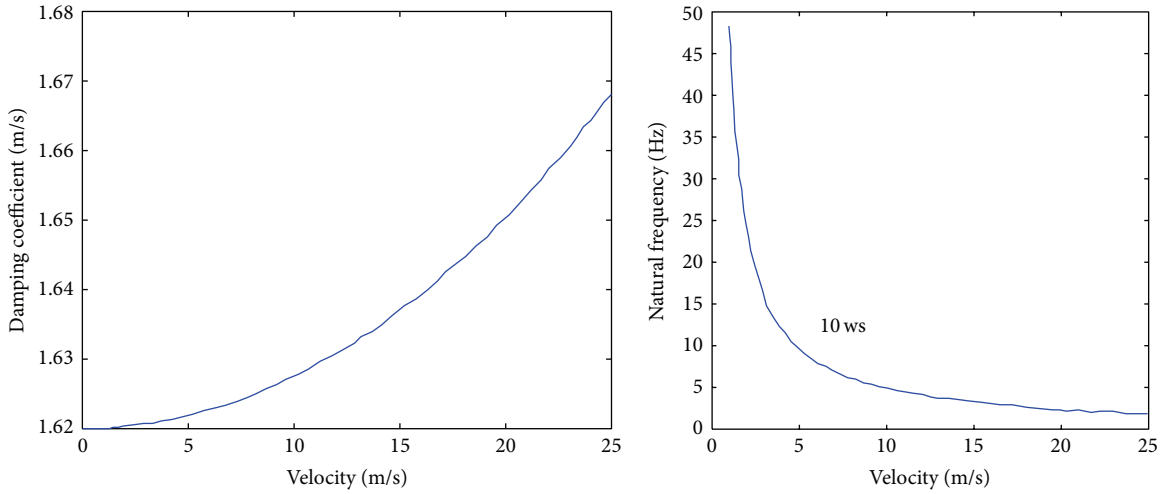

(a) The damping coefficient response (b) The natural frequency response

Figure 4: The vehicle response under different velocity.

where δ_0 is a constant value. The initial condition can be expressed as that $\omega(t) = 0$, $\delta_1 = \delta_0$, $\dot{\omega} = B_1\delta_0$.

We can get

$$A_1 = -\frac{B_0\delta_0}{\omega_0^2},$$
$$A_2 = \frac{B_0\delta_0}{\omega_0^2} * \left(\frac{B_1}{B_0}\omega_0^2 - \xi\omega_0\right) * \frac{1}{\omega_0\sqrt{1-\xi^2}}. \quad (15)$$

If the travelling velocity of the vehicle is 80 km/h, after the unit conversion to international standard unit, the region of u is (0 m/s, 25 m/s). The damping coefficient response and the natural frequency of the vehicle are shown in Figures 4(a) and 4(b). In Figure 4, the damping coefficient increases with the velocity and arrives at the maximum 1.67 m/s when the vehicle is 25 m/s. However the natural frequency decreases quickly with the velocity increase. When the vehicle velocity is more than 5 m/s, the natural frequency response is less than 10 Hz. The minimum value is nearly 2 Hz when the velocity is 25 m/s.

Combining the condition of velocity region and time region, we can get the yaw velocity gain as in Figure 5. The yaw velocity gain increases with the velocity firstly and then decreases. The peak value is nearly 1 when the velocity is 10 m/s.

3.2. The Electrohydraulic System Model. The electrohydraulic system mainly consists of the servo valve and the cylinder, as shown in Figure 6. The PWM signals from the controller are modified to change the current through the magnetic coil. Further, the displacement of the rod of valve core is controller. As a result, the hydraulic flow from and to the cylinder is consist with the reference value. The following is a summary of the assumption that has been made in developing the model of a hydraulic cylinder.

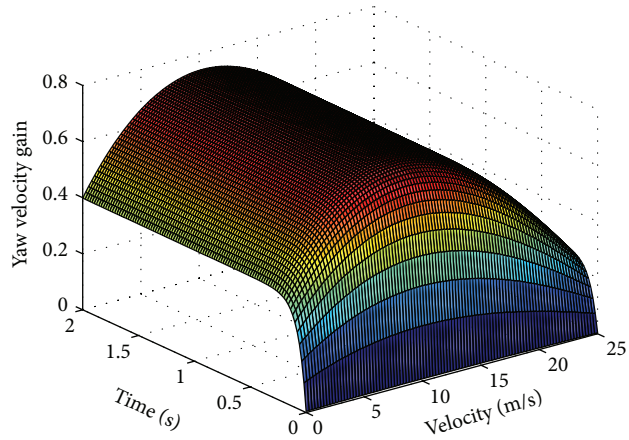

Figure 5: The yaw velocity gain of the vehicle.

(1) The proportional valve is a symmetrical 3-way and 4-port valve. The dead band of valve is also symmetrical, and the flow in it is turbulent.

(2) Possible dynamic behavior of the pressure in the transmission lines between valve and cylinder is assumed to be negligible.

(3) Pressure is equal everywhere in one volume of hydraulic cylinder, and the temperature and the bulk modulus are constants.

(4) The leakage of flows is laminar.

According to the continuous equation of compressible oil,

$$\sum Q_{\text{in}} - \sum Q_{\text{out}} = \frac{dV}{dt} + \frac{V}{\beta}\cdot\frac{dP}{dt}, \quad (16)$$

where V is the initial volume of liquid subjected to compression. dV and dP are the changes in pressure and volume,

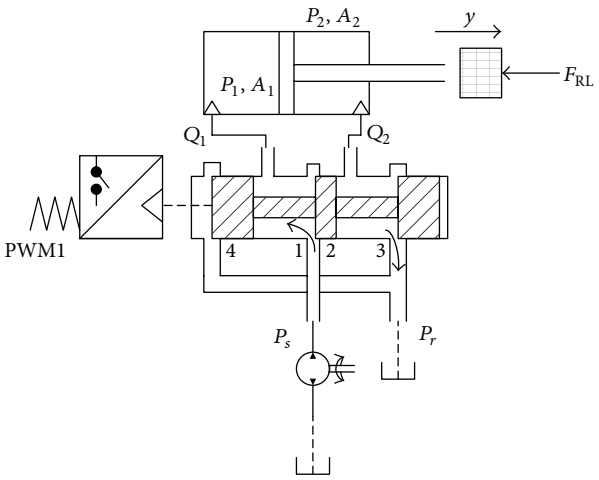

Figure 6: The diagram of hydraulic system after retrofitting.

respectively. $\sum Q_{in}$ is the input flows of liquid, and $\sum Q_{out}$ is the output flows of liquid. β is the bulk modulus.

Considering the internal and external leakage of a cylinder, the equations of the left and right chambers of a cylinder are defined as

$$\begin{aligned} Q_1 - C_{ic}(P_1 - P_2) - C_{ec}P_1 &= \frac{dV_1}{dt} + \frac{V_1}{\beta_e}\cdot\frac{dP_1}{dt}, \\ C_{ic}(P_1 - P_2) - Q_2 - C_{ec}P_2 &= \frac{dV_2}{dt} + \frac{V_2}{\beta_e}\cdot\frac{dP_2}{dt}, \end{aligned} \tag{17}$$

where Q_1 is the input flow to cylinder, and Q_2 is the output flows from cylinder, as shown in Figure 6. C_{ic} is the internal leakage coefficient. C_{ec} is the external leakage coefficient. β_e is the valid bulk modulus (including liquid and the air in the oil) and V_1, V_2 are the volume of fluid flow from and to the hydraulic cylinder.

V_1, V_2 can be got as follows:

$$\begin{aligned} V_1 &= V_{01} + A_1 y, \\ V_2 &= V_{02} - A_2 y, \end{aligned} \tag{18}$$

where V_{01} is the initial volume of cylinder side into where the fluid flows. V_{02} is the initial volume of cylinder side from which the fluid flows out. y is the displacement of piston.

So the derivation of (18) can be given as

$$\begin{aligned} \frac{dV_1}{dt} &= A_1\frac{dy}{dt}, \\ -\frac{dV_2}{dt} &= A_2\frac{dy}{dt}. \end{aligned} \tag{19}$$

Because of the development of sealing technology, the influence of external leakage can be neglected, which means the leakage between the piston rod and external seals. y can be expressed as a function of the wheel steering angle δ. Then (17) can be rebuilt as

$$\begin{aligned} \dot{P}_1 &= \frac{\beta_e}{V_1}\left[Q_1 - C_{ic}(P_1 - P_2) - A_1\frac{\partial y}{\partial \delta}\dot{\delta}\right], \\ \dot{P}_2 &= \frac{\beta_e}{V_2}\left[C_{ic}(P_1 - P_2) - Q_2 + A_2\frac{\partial y}{\partial \delta}\dot{\delta}\right], \end{aligned} \tag{20}$$

where C_{ic} is assumed to be a constant to simplify the system model.

The flow equation of electrohydraulic servo valve is that

$$\begin{aligned} Q_1 &= C_d W X_v \sqrt{\frac{2}{\rho}\Delta P_1} \\ &= \begin{cases} C_d W K_I I(t)\sqrt{\dfrac{2}{\rho}\Delta P}, & I(t) \geq 0, \\ -C_d W K_I I(t)\sqrt{\dfrac{2}{\rho}(P_1 - P_r)}, & I(t) < 0, \end{cases} \\ Q_2 &= C_d W X_v \sqrt{\frac{2}{\rho}\Delta P_2} \\ &= \begin{cases} -C_d W K_I I(t)\sqrt{\dfrac{2}{\rho}(P_2 - P_r)}, & I(t) \geq 0, \\ C_d W K_I I(t)\sqrt{\dfrac{2}{\rho}\Delta P}, & I(t) < 0, \end{cases} \end{aligned} \tag{21}$$

where P_r is the pressure of return oil. ΔP is the pressure of spring. C_d is the flow coefficient. W is the area grads of orifice. X_v is the displacement of spool. ρ is the density of oil. K_I is the current coefficient of the servo valve. $I(t)$ is the control current on the servo valve, which is proportional to the duty cycle of PWM signals.

There is some dead band in any servo valve, and C_d is proved to be nonlinear by experiment [18]. The valid displacement of spool can be given as follows:

$$x_{nav} = \begin{cases} x_v - x_d, & x_v \geq x_d, \\ 0, & -x_d \leq x_v \leq x_d, \\ x_v + x_d, & x_v < -x_d, \end{cases} \tag{22}$$

where x_d is the dead band of valve.

In Figure 7, the flow plus coefficient of valve can be approximated by two lines to simplify the model. To be controlled conveniently, Q (the flow of valve) can be expressed as

$$\begin{aligned} Q(x_v, \Delta P) &= Q_M(x_v, \Delta P) + \widetilde{Q}(x_v, \Delta P), \\ Q_{1M} &= C_{d1} W f_1(\Delta P_1)\, x_{nav}, \\ Q_{2M} &= C_{d2} W f_2(\Delta P_2)\, x_{nav}, \end{aligned} \tag{23}$$

where Q_M is the simplified projection function of flow. $\widetilde{Q}$ is the model error of the flow projection. Generally speaking, C_{d1} and C_{d2} are constant for a stable working state.

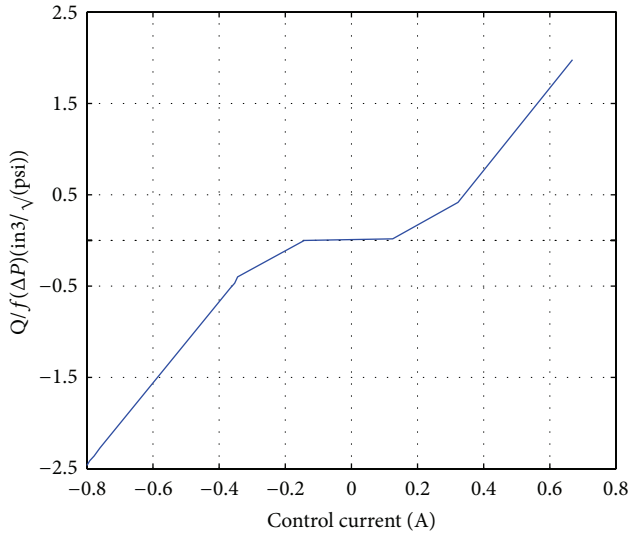

Figure 7: Nonlinear characteristic flow gain of the proportional valve.

According to the model of 4WS, the main difficulties to control are that (1) the system dynamics is strongly nonlinear and that (2) the system parameters are uncertain, for example, the uncertainty of m_L (inertia load), βe (valid bulk modulus), and T_n (the total disturb of system), which is brought by external disturb and unmodeled friction.

In this paper, the nonlinearity and uncertainty of parameters are treated by a robust controller. In Figure 7, the polyfit line is used to compensate for the dead band of the valve, which is the symmetrical line of plus curve based on the axis that is through the coordinate origin and makes an angle of 45 degrees with the x axis. The flow projection error is compensated by robust feedback. Then (16) and (20) can be transform to

$$\begin{aligned}
\ddot{\delta} &= \frac{q_1}{J_c}\left[x_L\left(P_1A_1 - P_2A_2\right) - G_c\left(\delta\right)\right] + \frac{q_1}{l_e^2}gl_g \\
&\quad - \frac{1}{l_e^2}gl_g + q_2 + \widetilde{T}\left(t,\delta,\dot{\delta}\right), \\
\dot{P}_1 &= \frac{q_3}{V_1}\left(-C_{\mathrm{ic}}\left(P_1 - P_2\right) - A_1\frac{\partial y}{\partial \delta}\dot{\delta} + Q_{1M} + \widetilde{Q}_1\right), \\
\dot{P}_2 &= \frac{q_3}{V_2}\left(A_2\frac{\partial y}{\partial \theta_2}\dot{\delta} - Q_{1M} - \widetilde{Q}_2\right) + C_{\mathrm{ic}}\left(P_1 - P_2\right),
\end{aligned} \tag{24}$$

where $q_1 = 1/(1 + (l_e/J_c)m_L)$, $q_2 = T_n/(J_c + m_Ll_e^2)$, $q_3 = \beta_e$, and $q = [q_1, q_2, q_3]^T$, $\widetilde{T} = (T(t,\delta,\dot{\delta}) - T_n)/(J_c + m_Ll_e^2)$, $q_{\min} \le q \le q_{\max}$, $|\widetilde{T}| \le \lambda_T$, $|\widetilde{Q}_1| \le \lambda_{Q1}$, $|\widetilde{Q}_2| \le \lambda_{Q2}$, and $q_{\min}$, $q_{\max}$, λ_T, and λ_{Q1}, λ_{Q2} are given value. It is assumed that $\widehat{q}$ and $\widetilde{q}$ are the estimated value and estimated error of q.

x_v is assumed to be proportional to $I(t)$; that is $x_v = KI(t)$; then

$$I\left(t\right) = Kx_v = \begin{cases} K\left(x_{nav} + x_d\right), & x_{nav} \ge 0, \\ 0, & x_{nav} = 0, \\ K\left(x_{nav} - x_d\right), & x_{nav} < 0. \end{cases} \tag{25}$$

4. Robust H_2/H_∞ Control

First, because the 4Ws system is composed of mechanical and electrical units, the coupling of two subsystems is a serious disturbance for the electrical control system. Secondly, the driver decisions are stochastic, resulting in the variation of certain parameters. Thirdly the stochastic variation of the pump pressure is uncertainty element for the model, so is the rolling resistance. On the other hand, the electrohydraulic system is a strongly nonlinear system for the inherent PWM modulation method and the dead band "born in nature," and the variation of parameters will deteriorate the system performance also. Considering the nonlinear and time-varying uncertainty of the steering system, robust H_2/H controller is put forward to guarantee both the system performance and the robust stability.

4.1. Robust H_2/H_∞ Control. A model in terms of state space equation is denoted as

$$\begin{aligned}
\dot{x} &= Ax + B_1u + B_2w, \\
z_1 &= C_1x + D_{11}u + D_{12}w, \\
z_2 &= C_2x + D_{21}u + D_{22}w,
\end{aligned} \tag{26}$$

where x is the state vector, u is the control input vector, w is the outer disturbance vector, z_1 and z_2 are the control output vector, and A, B_1, B_2, C_1, C_2, D_{11}, D_{12}, D_{21}, and D_{22} are known certain matrices defined by the nominal model. The robust H_2/H_∞ controller to be designed should guarantee that (1) the closed-loop system is stable; (2) the performance index for robustness satisfies that $\|T(z_1w)\|_\infty < \gamma_1$ with the parameter perturbation and outer disturbance, defined by the H_∞ norm of the transfer function $T(z_1w)$ from w to z_1; (3) the performance index for linear quadratic Gaussian (LQG) is as small as possible satisfying that $\|T(z_2u)\|_2 < \gamma_2$, defined by the H_2 norm of the transfer function $T(z_2u)$ from u to z_2. The design of the controller is meant to minimize γ_2 with the situation of $\sigma(A_c) \subset C^-$, $\|T_{z_1w}\|_\infty < \gamma_1$, $\|T_{z_2u}\|_2 < \gamma_2$, where K is the controller to be designed [19, 20].

To design the state feedback controller,

$$u = Kx. \tag{27}$$

Substituting (27) into (26),

$$\begin{aligned}
\dot{x} &= \left(A + B_1K\right)x + B_2w, \\
z_1 &= \left(C_1 + D_{11}K\right)x + D_{12}w, \\
z_2 &= \left(C_2 + D_{21}K\right)x + D_{22}w.
\end{aligned} \tag{28}$$

The robust hybrid controller design for (28) is difficult because of the solution of the nonlinear matrix inequality. According to the variable substitution method [21], the state feedback controller is solvable with the existence of the optimal solution X, W of (27). The robust hybrid controller can be expressed as (29),

$$u = WX^{-1}x,$$

$$\begin{aligned} &\min \ \gamma_2 \\ &\text{s.t.} \begin{cases} \begin{bmatrix} AX + B_1W + (AX + B_1W)^T & B_2 & (C_1X + D_{11}W)^T \\ B_2^T & -\gamma_1 I & D_{12} \\ C_1X + D_{11}W & D_{22} & -\gamma_1 I \end{bmatrix} < 0 \\ AX + B_1W + (AX + B_1W)^T + B_2B_2^T < 0 \\ \begin{bmatrix} -Z & C_2X + D_{21}W \\ (C_2X + D_{21}W)^T & -X \end{bmatrix} < 0 \\ \text{Trace}(z) < \gamma_2, \end{cases} \end{aligned} \tag{29}$$

where $z = [z_1 \ \ z_2]^T$.

4.2. The Proposed H_2/H_∞ Controller for 4WS. For the 4WS vehicle, Z_1 is defined as the yaw velocity of the vehicle ω. Z_2 is defined as the tire steering angle δ_{FL}, which is ratio to the sensor voltage. The sensor voltage is decided by the angular displacement of the steering wheel. Now define the performance index for robustness as the H_∞ norm of the sensitivity function from the parameter perturbation w to the control output z_1. Define the performance index for LQG as the H_2 norm of the transfer function from the control input U to the control output z_2. Then the state vectors $[X_1, X_2] = [\beta, \omega, P_1, P_2]$ are defined as the angles of the whole vehicle and the pressures of the hydraulic route, respectively. All the four state variables can be measured directly by physical sensor. So the state feedback controller is feasible [22, 23]. Now (29) is a convex optimization with LMI constraint and linear object function. The control system is made with the state variable feedback and a compensator, to track a step input with zero steady-state error. By solving the linear matrix inequality (29) with $\gamma_1 = 10$, $\gamma_2 = 12$ and setting the goal to achieve a settling time to be within 20% of the final value in less than 1 second and a deadbeat response while retaining a robust response, the compensator and state feedback controller are designed as

$$K = [0.096 \ \ 0.045 \ \ 0.089 \ \ 0.003]. \tag{30}$$

The controller can guarantee that the H_2 performance index is $\|T(z_2\mu)\|_2 < 12$ and the H_∞ index $\|T(z_1\omega)\|_\infty < 10$. The nominal closed-loop model is robust with its gain margin 38 dB and phase margin 52 deg with the designed controller. The continuous transfer function of the controller is shown in

$$K(s) = \frac{47s^2 + 107s}{2s^3 + 32s^2 + 527s + 165}. \tag{31}$$

A linear continuous model control system is stable if all poles of the closed-loop transfer function $T(s)$ lie in the left half of the s-plane. The z-plane is related to the s-plane by the transformation $z = e^{sT} = e^{(\sigma + j\omega)T}$. In the left-hand s-plane, $\sigma < 0$, and therefore the related magnitude of z varies between 0 and 1. Therefore the imaginary axis of the s-plane corresponds to the unit circle in the z-plane, and the inside of the unit circle corresponds to the left half of the s-plane. Therefore we can state that a sampled system is stable if all the poles of the closed-loop transfer function $T(z)$ lie within the unit circle of the z-plane, as shown in Figure 8.

The discretization/interpolation methods include zero-order hold, first-order hold, impulse invariant mapping, bilinear approximation, and matched poles and zeros [24, 25]. The zero-order hold and first-order hold methods are generally accurate for systems driven by smooth inputs. For the PWM modulation system, the impulse invariant mapping and the bilinear transform methods are used. The impulse invariant mapping matches the discretized impulse response with that of the continuous time system. Note that the impulse responses match and the frequency responses do not match, however, because of the scaling factor T_s, the sample time. Although the impulse invariant transform is ideal when you are interested in matching the impulse response, it may not be a good choice if you are interested in matching the frequency response of the continuous system, because it is susceptible to aliasing. As the sampling time increases, you can see the effects of aliasing. In general, if you are interested in matching the frequency response of the continuous system, a bilinear transform (such as Tustin approximation) is a better choice. So the bilinear transform method is selected here. Choosing the right sample time involves many factors, including the performance, the fastest time constant, and the running speed. With the sample time $T_s = 5$ ms, the controller by bilinear transform is shown in (32). The discrete system is stable:

$$H_d(z) = \frac{0.5817z^3 - 0.5783z^2 - 0.5783z + 0.5817}{z^3 - 1.623z^2 + 0.8637z - 0.2308}, \tag{32}$$

$$p1 = 0.9830, \qquad p2 = 0.3199 + 0.3639i,$$

$$p3 = 0.3199 - 0.3639i. \tag{33}$$

5. The Experiment

First the control hardware is introduced. Then the experiments are carried out, including two aspects, the time domain response and the frequency domain experiments. At last the analysis is given out.

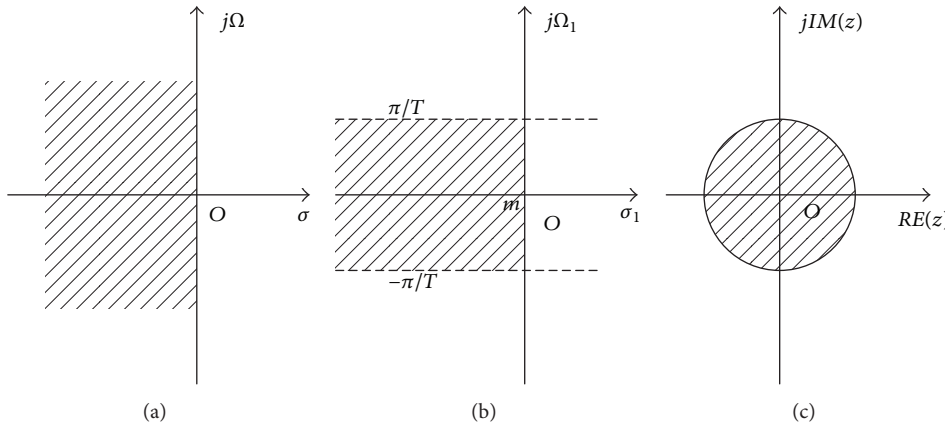

Figure 8: The bilinear transformation.

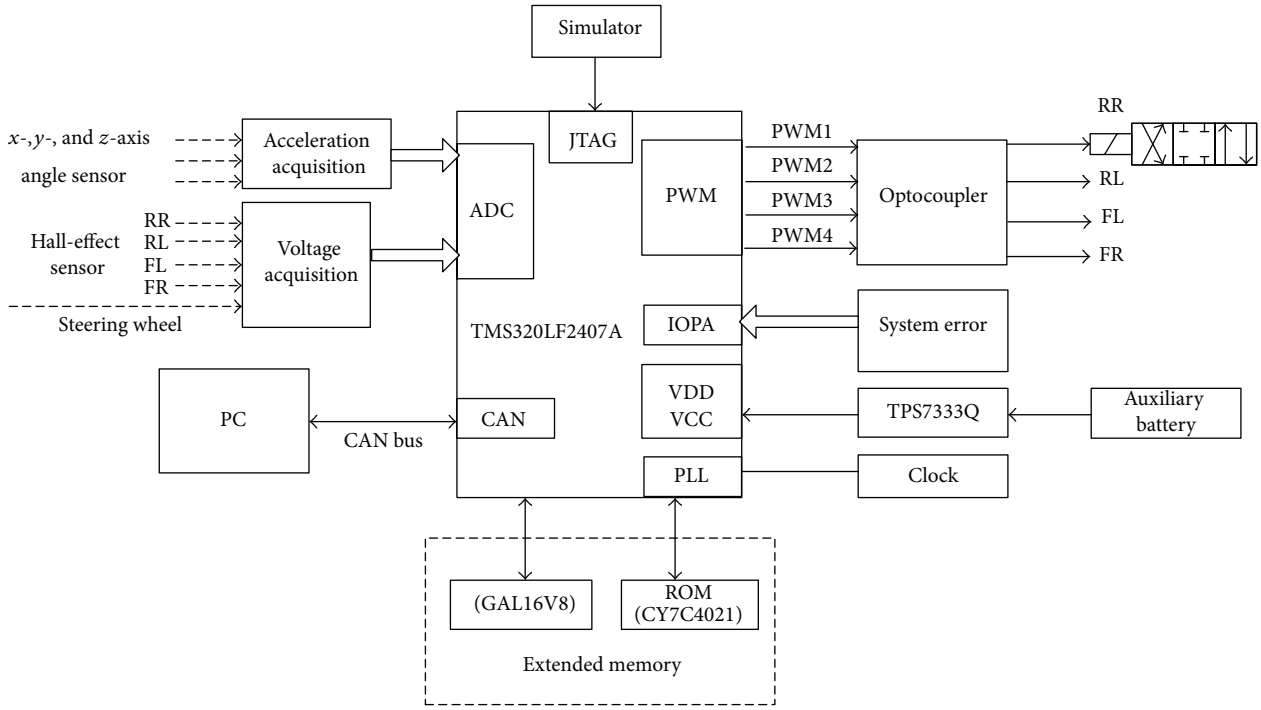

Figure 9: The control diagram based on DSP.

5.1. The Hardware Controler for 4WS. The configuration of the hardware controller for 4WS is shown in Figure 9. In the experimental implementation, the required time for the controller to execute all the tasks is approximately 60 ms during one period. Designer always moved to a DSP when the application requires a great deal of mathematical computations since the DSPs perform calculations faster than the single chip controller. The core processor of the experimental system is a DSP TMS320LF2407 with clock frequency of 40 MHz, produced by TI Company. The servo valve is driven by a voltage-fed PWM converter with a switching frequency of 200 Hz. The angles of each wheel are detected by the Hall-Effect device and the detected analogue signals are converted to digital values by using the A/D converter with a 12-bit resolution. The discrete controller is programmed by C language and loaded into the DSP.

5.2. The Time Domain Experiments. The standard velocity is 80 km/h, the acceleration velocity of the steering wheel is as quick as possible, and it is better more than 200 degree/sec. The driver turned the steering wheel to the left 80 degrees and then to the right 80 degrees. Then return to 0 degrees. Repeat

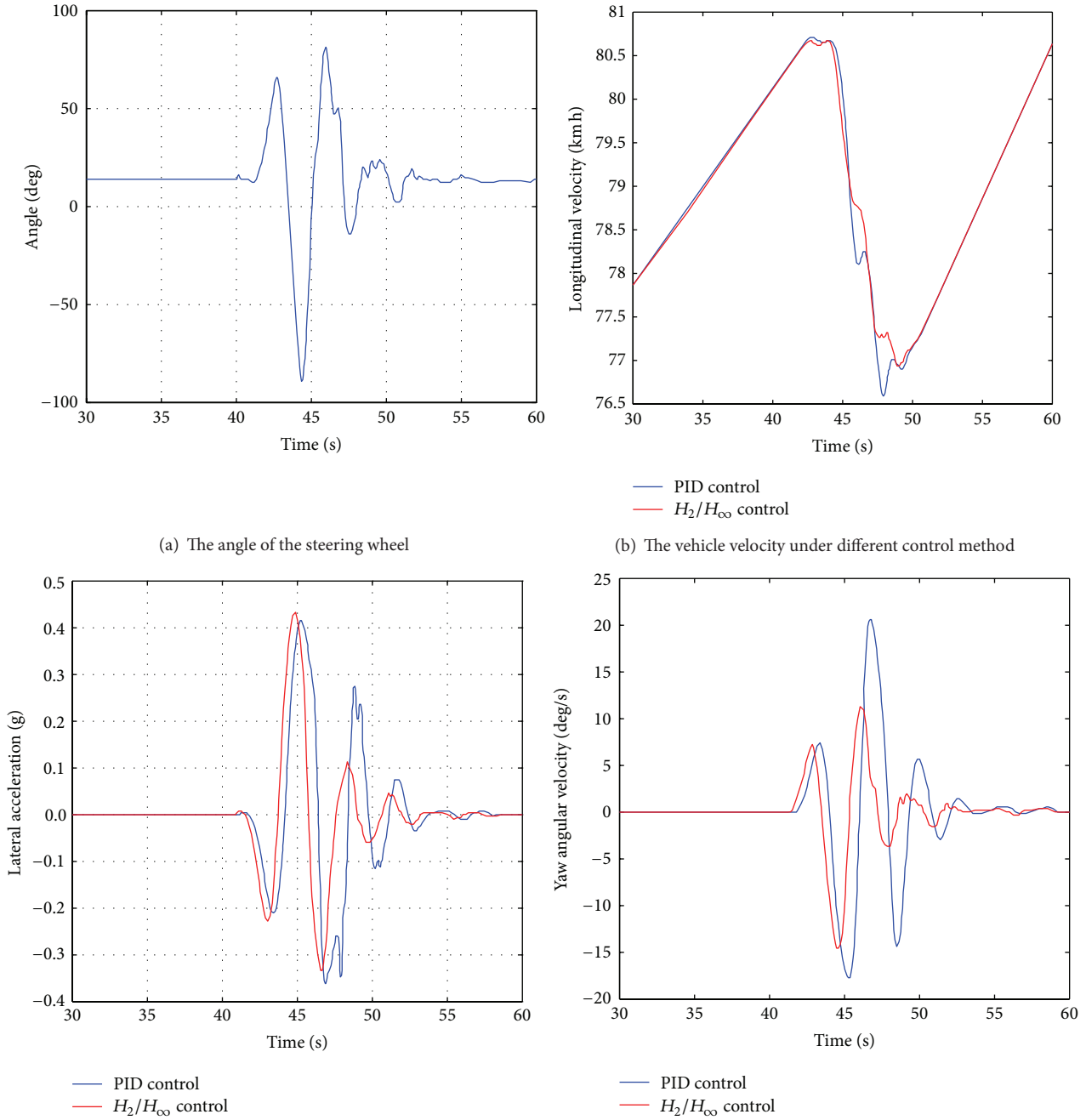

(a) The angle of the steering wheel

(b) The vehicle velocity under different control method

(c) The lateral acceleration comparison

(d) The yaw velocity comparison

Figure 10: The time domain experimental results.

for another time. The steering time is 3 s at least; then release the steering wheel. During the experiments the accelerator pedal should be kept constant to decrease the affection of the engine velocity fluctuating. The input reference of the steering wheel is shown in Figure 10(a); the steering wheel is acted at 40 s. After the vehicle is fired, the vehicle velocity can be stable after 30 s. Hold on about 10 s and then release the steering wheel. The comparisons of the vehicle velocity, the lateral acceleration, and the yaw velocity under different control methods are shown in Figures 10(b), 10(c), and 10(d), respectively.

From Figure 10(a), we can see there is some dead band for the steering wheel, which is nearly 10 degrees. It is normal for a vehicle. In Figure 10(b), the vehicle velocity is nearly the same during the steering. The vehicle velocity decreases during the steering process. However, the velocity fluctuating is smaller by the H_2/H_∞ controller compared to that of the PID control method. From Figure 10(c), the change law of the lateral acceleration is the same for two control methods. We can conclude that the H_2/H_∞ controller is superior to PID in that the responding time is quicker and the stable time is shorter. In Figure 10(d), obviously the yaw velocity

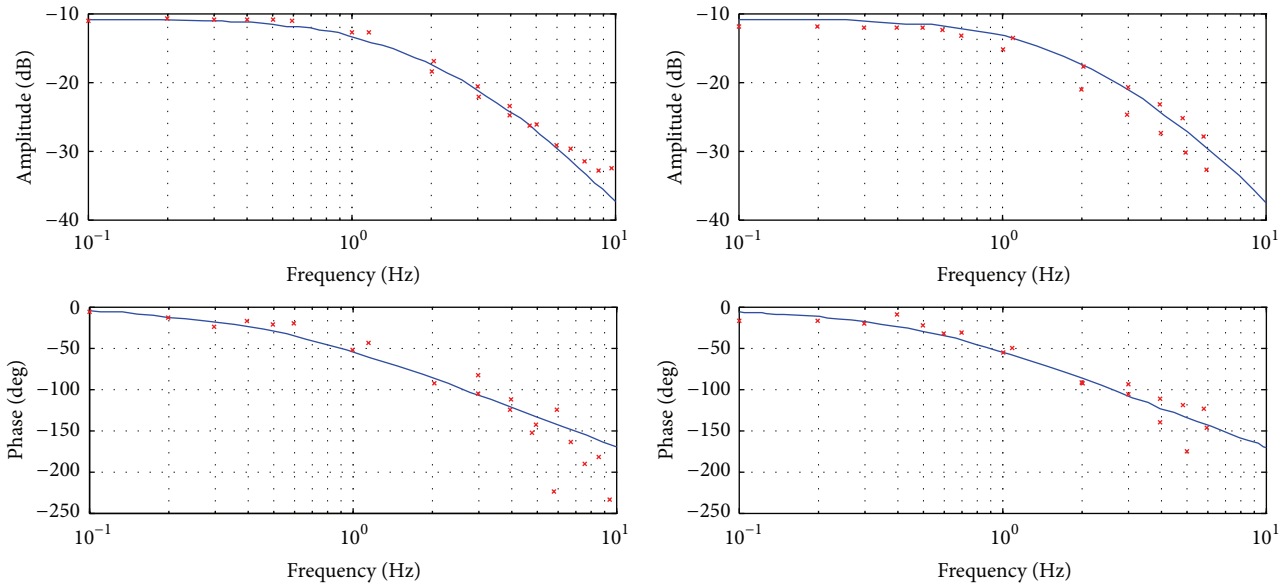

(a) Robust H_2/H_∞ control

(b) PID control

FIGURE 11: Fitted bode plot from experimental results.

is better than that of PID; the maximum value is only 11 degree/sec; however the maximum value is more than 20 degree/sec. The performance can be improved nearly 40%. So the effectiveness of 4ws and the superiority of the robust control method are validated.

5.3. The Frequency Domain Experiments. Furthermore, the experiments are carried out on the 4WS vehicle. The outputs are the steering angle signals from hall-effect sensor of four wheels. Both the input and output signals are recorded by the tape recorder. Then the test results are analyzed by the HP3562 signal analyzer. Focus on a particular frequency region [0.1 Hz, 10 Hz]. The input signals are composed of the direct current signals of amplitude 2.5 V and the alternating current signals of amplitude 0.5 V. The input frequency changes from 0.1 Hz to 0.6Hz at the interval of 0.1 Hz and then changes from 1 Hz to 10 Hz at the interval of 1 Hz.

The closed-loop bode plots of the 4WS are fitted from experimental results. Figure 11(a) showed the plot under the proposed H_2/H_∞ controller. The bode plot under PID control is shown in Figure 11(b). With the outer disturbance, the control performance is bad under PID control, as for that a lot of experimental data is far away from the theoretical transform function and the amplitude of output signals can arrive at the predefined value. The consequences of the steering angle are bad, especially when the frequency of input signal is higher than 6 Hz; the output signals are so small that it cannot be plotted in the defined range. However for the proposed H_2/H_∞ controller, the experimental results are satisfied with the fact that the data are consistent with the theoretical transfer function. For the high frequency input, the control performance is still good. The control performance and robustness of the steering system can be guaranteed by the proposed H_2/H_∞ controller, which is superior to classical PID controller.

6. Conclusion

The principle and scheme of a 4WS vehicle are depicted in the paper, coupled with mechanism-hydraulic-electric subsystem. The construction and working principle are depicted in detail. To attenuate the uncertainty system with the variation of the system parameters, the driver decision, and the road condition, the robust H_2/H_∞ control was put forward. The proposed scheme was designed by Matlab toolbox and then implemented by microcontroller DSP. The experimental results showed that the proposed scheme was endowed with good dynamic performance and robust stability. The yaw velocity can be improved by 40% at least by the robust H_2/H_∞ controller. The experiment results showed that the proposed controller is effective to guarantee the accuracy, celerity, stability, and robustness of the steering system.

Conflict of Interests

The authors declare that there is no conflict of interests regarding the publication of this paper.

Acknowledgments

The project was supported by the National Natural Science Foundation of China (no. 51105043) and Special Fund for Basic Scientific Research of Central Colleges, Chang'an University (CHD2011ZD016). The authors would like to express their thanks for the funds provided.

References

[1] T. H. Akita and K. H. Satoh, "Development of 4WS control algorithms for an SUV," *JSAE Review*, vol. 24, no. 4, pp. 441–448, 2003.

[2] K. H. Guo and H. Ya, "Progress in controlling methods of four wheel steering system," *Journal of Jilin University of Technology*, vol. 28, no. 4, pp. 1–4, 1998.

[3] M. Ye, B. G. Cao, and G. M. Si, "Study on the control platform of four wheel steering," *China Mechanical Engineering*, vol. 18, no. 13, pp. 1625–1628, 2007.

[4] Q. Z. Qu and Y. Z. Liu, "The review and prospect of four-wheel-steering research from the viewpoint of vehicle dynamics and control," *China Mechanical Engineering*, vol. 10, no. 8, pp. 946–949, 1999.

[5] Y. M. Jia, "Robust control with decoupling performance for steering and traction of 4ws vehicles under velocity varying motion," *IEEE Transactions on Control Systems Technology*, vol. 8, no. 5, pp. 554–569, 2000.

[6] K. M. Passino and S. Yurkovich, *Fuzzy Control*, Addison-Wesley, New York, NY, USA, 1997.

[7] M. Nishida and M. Sugeno, "Fuzzy control of model car," *Fuzzy Sets and Systems*, vol. 60, no. 6, pp. 103–113, 1985.

[8] J. Ackermann and W. Sienel, "Robust yaw damping of cars with front and rear wheel steering," *IEEE Transactions on Control Systems Technology*, vol. 1, no. 1, pp. 15–20, 1993.

[9] X. Ji, H. Su, and J. Chu, "Robust state feedback $H\infty$ control for uncertain linear discrete singular systems," *IET Control Theory & Applications*, vol. 1, no. 1, pp. 195–200, 2007.

[10] H.-M. Lv, N. Chen, and P. Li, "Multi-objective H_∞ optimal control for four-wheel steering vehicle based on a yaw rate tracking," *Proceedings of the Institution of Mechanical Engineers, Part D: Journal of Automobile Engineering*, vol. 218, no. 10, pp. 1117–1124, 2004.

[11] S.-S. You and Y.-H. Chai, "Multi-objective control synthesis: an application to 4WS passenger vehicles," *Mechatronics*, vol. 9, no. 4, pp. 363–390, 1999.

[12] X. G. Yan, S. K. Spurgeon, and C. Edwards, "Static output feedback sliding mode control for time-varying delay systems with time-delayed nonlinear disturbances," *International Journal of Robust and Nonlinear Control*, vol. 20, no. 7, pp. 777–788, 2010.

[13] X.-G. Yan, C. Edwards, and S. K. Spurgeon, "Decentralised sliding-mode control for multimachine power systems using only output information," *IEE Proceedings—Control Theory and Applications*, vol. 151, no. 5, pp. 627–635, 2004.

[14] J. Chen, N. Chen, G. Yin, and Y. Guan, "Sliding-mode robust control for a four-wheel steering vehicle based on nonlinear characteristic," *Journal of Southeast University*, vol. 40, no. 5, pp. 969–972, 2010.

[15] J. C. Doyle, K. Glover, P. P. Khargonekar, and B. A. Francis, "State-space solutions to standard H_2 and H_∞ control problems," *IEEE Transactions on Automatic Control*, vol. 34, no. 8, pp. 831–847, 1989.

[16] K. Glover and D. McFarlane, "Robust stabilization of normalized coprime factor plant descriptions with H_∞-bounded uncertainty," *IEEE Transactions on Automatic Control*, vol. 34, no. 8, pp. 821–830, 1989.

[17] F. Fahimi, "Full drive-by-wire dynamic control for four-wheel-steer all-wheel-drive vehicles," *Vehicle System Dynamics*, vol. 51, pp. 360–376, 2013.

[18] A. Ghaffari, S. Hamed Tabatabaei Oreh, R. Kazemi, and M. A. Reza Karbalaei, "An intelligent approach to the lateral forces usage in controlling the vehicle yaw rate," *Asian Journal of Control*, vol. 13, no. 2, pp. 213–231, 2011.

[19] B. A. Güvenç, L. Güvenç, and S. Karaman, "Robust MIMO disturbance observer analysis and design with application to active car steering," *International Journal of Robust and Nonlinear Control*, vol. 20, no. 8, pp. 873–891, 2010.

[20] Y.-D. Song, H.-N. Chen, and D.-Y. Li, "Virtual-point-based fault-tolerant lateral and longitudinal control of 4W-steering vehicles," *IEEE Transactions on Intelligent Transportation Systems*, vol. 12, no. 4, pp. 1343–1351, 2011.

[21] G. D. Yin, N. Chen, J. X. Wang, and J. S. Chen, "Robust control for 4WS vehicles considering a varying tire-road friction coefficient," *International Journal of Automotive Technology*, vol. 11, pp. 33–40, 2010.

[22] G.-D. Yin, N. Chen, J.-X. Wang, and L.-Y. Wu, "A study on μ-synthesis control for four-wheel steering system to enhance vehicle lateral stability," *Journal of Dynamic Systems, Measurement, and Control*, vol. 133, no. 1, Article ID 011002, 2011.

[23] R. Marino and S. Scalzi, "Asymptotic sideslip angle and yaw rate decoupling control in four-wheel steering vehicles," *Vehicle System Dynamics*, vol. 48, pp. 999–1019, 2010.

[24] L. Menhour, D. Lechner, and A. Charara, "Two degrees of freedom PID multi-controllers to design a mathematical driver model: experimental validation and robustness tests," *Vehicle System Dynamics*, vol. 49, pp. 595–624, 2011.

[25] K. F. Zheng, S. Z. Chen, and Y. Wang, "Four-wheel steering with total sliding mode control," *Journal of Southeast University*, vol. 43, no. 2, pp. 334–339, 2013.